CHIN. PHYS. LETT. Vol. 38, No. 9 (2021) 090302

Reverse Rotation of Ring-Shaped Perturbation on Homogeneous Bose–Einstein Condensates

Peng Gao(高鹏)[1,2], Zeyu Wu(吴泽宇)[3], Zhan-Ying Yang(杨战营)[1,2,4*], and Wen-Li Yang(杨文力)[1,2,4,5]

[1]*School of Physics, Northwest University, Xi'an 710127, China*
[2]*Shaanxi Key Laboratory for Theoretical Physics Frontiers, Xi'an 710127, China*
[3]*Department of Physics and Astronomy, University College London, London WC1E 6BT, UK*
[4]*Peng Huanwu Center for Fundamental Theory, Xi'an 710127, China*
[5]*Institute of modern Physics, Northwest University, Xi'an 710127, China*

(Received 27 June 2021; accepted 30 July 2021; published online 2 September 2021)

We numerically study the dynamics of rotating ring-shaped perturbation on two-dimensional homogeneous Bose–Einstein condensates, where a new ring-shaped structure with reverse rotation appears. The reversely rotating mode is directly caused by the existence of the plane wave (namely the homogeneous background). By the modified linear stability analysis method, we quantitatively predict the influence of the background's density on perturbation dynamics, including the velocity, amplitude, and frequency of the two rings. We construct an approximative solution to describe the short-lived dynamics of initial perturbation, which agrees well with our numerical results. Also, after the two rings separate, the transfer of atom number between them becomes linear, and the rate of transfer is impacted by the radial momentum of initial perturbation.

DOI: 10.1088/0256-307X/38/9/090302

Bose–Einstein condensates (BECs) have been attracting much attention over the last century, providing a good platform for observation of localized structures including solitons.[1–5] The dynamics of BECs can be well described by the Gross–Pitaevskii (GP) model with the mean-field approximation.[6] Considering only the contact interaction of atoms, the 1D GP model became integrable, and so prompted a large amount of research on exact solutions of waves. These waves can be classified into many categories according to their dynamical features and stability, including solitons,[7–10] rogue waves,[11–17] breathers,[18–23] and so on.[24] Most of them inherently require the presence of plane wave background, which created inspiration to generate them by perturbing a plane wave. For example, the step-type perturbations on a phase were used for generating dark solitons;[25] the periodic- or localized-type perturbations lead to an Akhmediev breather or rogue wave generations.[26,27] Thus, much effort has been made for dynamics of a 1D perturbed plane wave.[28–32]

In the multi-dimensional BECs, the collapse instability and non-integrability of the model brings great difficulty for the wave generations.[6,33,34] However, in some studies of multi-dimensional non-GP models, the perturbations have been expressed as interesting dynamical behaviors, like the pseudorecurrence of modulation stability[35] and even the rogue wave generations.[36–38] It was indicated that the perturbations may manifest abundant but little-known dynamics in multi-dimensional BECs. In 2D attractive BECs, a transversely periodic perturbation could induce modulation instability. Unlike the 1D case, the induced modulation instability is followed by the collapse dynamics of density peaks. Also, the periodicity of perturbation can be initially set in the angular direction.[39] One of the typical perturbations is the rotating ring-shaped one, whose stability is greatly affected by its angular momentum. When the atomic interaction turns into a repulsive type, this perturbation's instability vanishes and its expansion dynamics dominates. Especially, it is found that a new ring with reverse rotation emerges during the expansion. This novel phenomenon differs from the previous dynamics of perturbation, so this deserves careful study.

In this Letter, we numerically study the dynamics of rotating ring-shaped perturbation on plane waves in two-dimensional BECs. A new ring-shaped structure appears and rotates towards the reverse direction. The amplitude of derived ring gets larger when the amplitude of the plane wave increases, so its emergence may benefit from the presence of the plane wave background. We predict the quantitative dynamical features of two rings and construct an approximative solution to describe the evolution of perturbation, which agrees well with the numerical results. Meanwhile, the linear transfer of atoms between two rings occurs after they separate. With different initial sets

Supported by the National Natural Science Foundation of China (Grant Nos. 11875220 and 12047502).
*Corresponding author. Email: zyyang@nwu.edu.cn
© 2021 Chinese Physical Society and IOP Publishing Ltd

of radial momentum, the transfer rate of atoms will change obviously.

Model and Dynamics of Ring-Shaped Perturbation. The dynamics of BECs can be described by the Gross–Pitaevskii model as follows:[6]

$$i\hbar\partial_t\Psi = -\frac{\hbar^2}{2\,m}\nabla^2\Psi + V_{\rm ext}(\boldsymbol{r})\Psi + g|\Psi|^2\Psi, \quad (1)$$

where $\Psi(\boldsymbol{r},t)$ is the mean-field wave function of condensates. The strength of contact interaction is $g = 4\pi\hbar^2 a_{\rm s}/m$ with the atom mass m and the s-wave scattering length $a_{\rm s}$. The external potential $V_{\rm ext}(\boldsymbol{r})$ provides a trap in which the condensates are confined, and it can be assumed as a harmonic form $V_{\rm ext}(\boldsymbol{r}) = m\omega_z^2 z^2/2$, with ω_z being the axial trapping frequency. Here, the transverse trap is neglected. In the axial external trap $V_{\rm ext}(\boldsymbol{r})$, the condensates are compressed to be pancake-shaped and can be considered as quasi-2D BECs. An effective way to reduce the model (1) into the 2D type is to assume the wave function $\Psi(\boldsymbol{r},t) = \psi(x,y,t)\phi(z)\exp(-i\omega_z t/4)$, where $\phi(z) = \exp(-z^2/2l_z^2)/(\pi^{1/4}\sqrt{l_z})$ and $l_z = \sqrt{\hbar/m\omega_z}$. By the integration over axial directions, the 2D model can be obtained,

$$i\hbar\partial_t\psi = -\frac{\hbar^2}{2\,m}(\partial_x^2\psi + \partial_y^2\psi) + \frac{g}{\sqrt{2\pi}l_z}|\psi|^2\psi. \quad (2)$$

Then, by the transformation

$$t \to \frac{1}{\omega_z}\,t,\ x \to l_z\,x,\ y \to l_z\,y,\ \psi \to \frac{1}{\sqrt[4]{8\pi}}\frac{1}{\sqrt{l_z\,a_{s0}}}\psi,$$

we can transform the 2D model into a dimensionless one,

$$i\psi_t = -\frac{1}{2}(\psi_{xx} + \psi_{yy}) + \tilde{g}|\psi|^2\psi, \quad (3)$$

where the subscripts denote the corresponding derivatives. We have $\tilde{g} = a_{\rm s}/a_{s0}$ to scale the contact interaction of atoms, and $a_{s0} > 0$ is the adjustable background value of scattering length. The positive (or negative) value of $\tilde{g}$ indicates the repulsive (or attractive) interaction. Here, we consider the case of $a_{s0} = a_{\rm s}$, i.e., $\tilde{g} = 1$, which corresponds to the repulsive contact interaction of atoms. In the polar coordinates (r,θ), the model becomes

$$i\psi_t + \frac{1}{2}\left(\frac{1}{r}\psi_r + \psi_{rr} + \frac{1}{r^2}\psi_{\theta\theta}\right) - |\psi|^2\psi = 0. \quad (4)$$

The relations between two coordinates are $x = r\cos\theta$ and $y = r\sin\theta$. In the model (4), a plane wave solution exists:

$$\psi_0(r,\theta,t) = a_0 e^{-i\,a_0^2\,t}, \quad (5)$$

where a_0 is the amplitude of plane wave. In real BECs, the plane wave state can be constructed by transversely trapping the condensates in a flat-bottom external potential. In addition, one can also use the background wave with a Gaussian type, which is located in an external harmonic trap. When its width is much larger than the perturbation's, it can be considered as a plane wave with space-dependent density in our analysis, and the phenomena mentioned in this study can also be observed on this background wave.

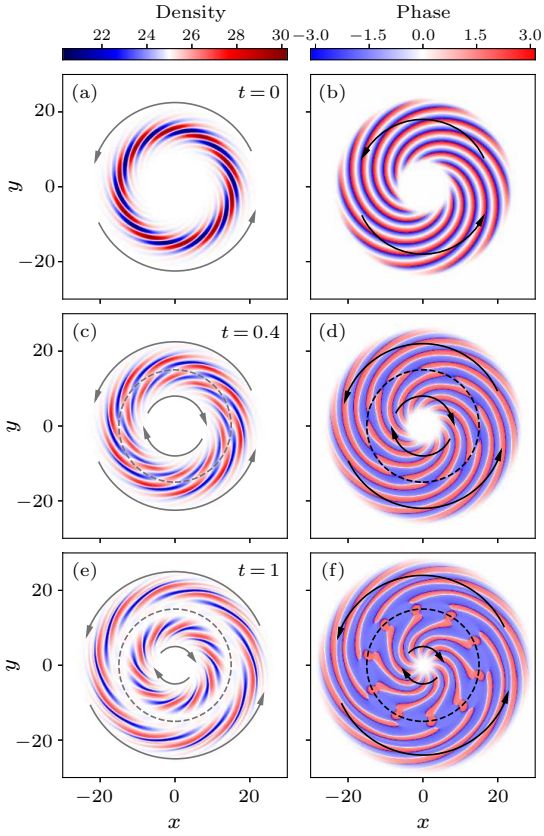

Fig. 1. Density distributions of initial condition (6) at (a) $t = 0$, (c) $t = 0.4$, (e) $t = 1$; and their corresponding phase distributions in (b), (d), and (f), respectively. The arrows denote the rotating direction of rings, not including the contribution of radial motion. The dashed circle is $r = r_0$. The perturbation splits into two rings with reverse rotating directions. The parameters are $a_0 = 5$, $a = 0.5$, $r_0 = 15$, $\eta_{(r)} = 1$, $k_{(r)} = 2$, $k_{(\theta)} = 10$.

Let us focus on the dynamics of rotating ring-shaped perturbation on the plane wave. The ring-shaped solitons in 2D BECs have been studied, which need an axial rotation to stabilize themselves.[40] Referring to their mathematical form, we define the initial condition by

$$\psi(r,\theta,0) = a_0 + a\,\mathrm{sech}[\eta_{(r)}(r - r_0)] \cdot \exp[ik_{(r)}r + ik_{(\theta)}\theta], \quad (6)$$

where a is the amplitude of perturbation, and r_0 is the radius of the ring. The localization of the ring is described by $\eta_{(r)}$, which scales the ring's thickness. Here $k_{(r)}$ and $k_{(\theta)}$ are the radial momentum and angular momentum, respectively. The parameters are set as $a_0 = 5$, $a = 0.5$, $r_0 = 15$, $\eta_{(r)} = 1$, $k_{(r)} = 2$, $k_{(\theta)} = 10$.

By the split-step Fourier method,[41] the distributions of density and phase at different times can be obtained numerically. The density is measured by $|\psi|^2$ while the phase is measured by $\varphi = \mathrm{Arg}[\psi \exp(ia_0^2 t) - a_0]$ to neglect the influence of background. The gradient of phase represents the flow velocity of atoms, namely $v_{\mathrm{atom}} = \nabla\varphi$, so the flow direction of atoms can be deduced by the phase distribution. When $t = 0$, the initial density and phase distributions are shown in Figs. 1(a) and 1(b), respectively. There is a counterclockwise rotating ring on the plane wave background. When $t = 0.4$, the initial ring splits into two close rings with opposite rotating directions, which are divided by the circle $r = r_0$, as shown in Figs. 1(c) and 1(d). When $t = 1$, the two rings separate obviously, as shown in Figs. 1(e) and 1(f). One of them has an increasing radius while the other has a decreasing one. We take the condensates of ^{85}Rb as an example. The atom mass is $m = 1.4 \times 10^{-25}$ kg, and one can experimentally set the axial trapping frequency $\omega_z = 2\pi \times 150$ Hz. Thus, the units of time and space are $t_{\mathrm{u}} = 1/\omega_z = 1\,\mathrm{ms}$ and $r_{\mathrm{u}} = l_z = 2.23\,\mu\mathrm{m}$, respectively. The realistic radius of initial perturbation is $r_{\mathrm{u}} r_0 = 33.5\,\mu\mathrm{m}$. The observation time of this phenomenon is limited to the range from 1 ms to 3 ms, which prevents the shrinking ring-shaped structure reaching the coordinate center. In the following, the reverse rotation dynamics of ring-shaped perturbation will be analyzed detailedly.

Dynamical Analysis of Perturbed Homogeneous Condensates. We recall that the perturbation in the initial condition (6) possesses both periodicity and localization. Therefore, its quantitative dynamics can be predicted by the modified linear stability analysis.[42,43] This method can provide many quantitative dynamical features of perturbation on the plane wave, including its periodicity, localization, and velocity. It starts with an ansatz of a perturbed plane wave,

$$\psi(r, \theta, t) = \psi_0[1 + u(r, \theta, t)], \tag{7}$$

where u is the perturbation with condition $|u| \ll 1$. Substituting Eq. (7) into the model (4) and linearizing it, the linear equation about u can be obtained as follows:

$$iu_t + \frac{1}{2}\Big(\frac{1}{r}u_r + u_{rr} + \frac{1}{r^2}u_{\theta\theta}\Big) - a_0^2(u + u^*) = 0. \tag{8}$$

Then, we assume that the perturbation has the form

$$u = Ae^{p(r,\theta,t)} + Be^{p^*(r,\theta,t)}, \tag{9}$$

where p is a complex function describing the features of perturbation, A and B are the amplitudes of two conjugate components. Substituting Eq. (9) into Eq. (8), one can obtain a set of two homogeneous equations for A and B^*,

$$\begin{bmatrix} c_{11} & c_{12} \\ c_{21} & c_{22} \end{bmatrix} \begin{bmatrix} A \\ B^* \end{bmatrix} = 0, \tag{10}$$

where

$$\begin{aligned} c_{11} &= ip_t - a_0^2 + \frac{M}{2r^2}, \quad c_{12} = -a_0^2, \\ c_{21} &= -a_0^2, \quad c_{22} = -ip_t - a_0^2 + \frac{M}{2r^2}, \\ M &= p_\theta^2 + p_{\theta\theta} + rp_r + r^2p_r^2 + r^2p_{rr}. \end{aligned}$$

The existence of a nontrivial solution of A and B^* requires only the determinant of the coefficient matrix equal to 0. It leads to

$$p_t = \pm\frac{1}{2r^2}\sqrt{M(4a_0^2r^2 - M)}. \tag{11}$$

Comparing the initial condition (6) and Eq. (9), when $B = 0$, the relation between p and the initial perturbation is

$$p = \ln\big\{\mathrm{sech}[\eta_{(r)}(r - r_0)]\big\} + ik_{(r)}r + ik_{(\theta)}\theta.$$

By this relation, the initial expressions of p_r, p_{rr}, p_θ, and $p_{\theta\theta}$ can be given. Note that the angle coordinate θ in the function p_t is eliminated in this case, namely, p_t is isotropic on the direction of θ.

Next, we focus on the analysis of dynamical features of perturbation. In the polar coordinates (r, θ), its periodicity and localization in the direction of space are, respectively, expressed as

$$\begin{aligned} \boldsymbol{K} &= [K_{(r)}, K_{(\theta)}] = (\mathrm{Im}[p_r], \mathrm{Im}[p_\theta]), \\ \boldsymbol{H} &= [H_{(r)}, H_{(\theta)}] = (\mathrm{Re}[p_r], \mathrm{Re}[p_\theta]), \end{aligned} \tag{12}$$

where Im and Re means the imaginary and real parts of complex functions. The perturbation's frequency and localization on the direction of time are, respectively, described by

$$\Omega = -\mathrm{Im}[p_t], \quad G = -\mathrm{Re}[p_t]. \tag{13}$$

The perturbation's periodicity expresses as the interference fringes between the background and the perturbation itself, while its localization expresses as the envelopes on the plane wave background (see Fig. 1). Hence, the velocities of fringes and envelopes are, respectively,

$$\begin{aligned} \boldsymbol{V} &= [V_{(r)}, V_{(\theta)}] = \Big[\frac{\Omega}{K_{(r)}}, \frac{\Omega}{K_{(\theta)}}\Big] \\ &= \Big(-\frac{\mathrm{Im}[p_t]}{\mathrm{Im}[p_r]}, -\frac{\mathrm{Im}[p_t]}{\mathrm{Im}[p_\theta]}\Big), \\ \boldsymbol{\Lambda} &= [\Lambda_{(r)}, \Lambda_{(\theta)}] = \Big[\frac{G}{H_{(r)}}, \frac{G}{H_{(\theta)}}\Big] \\ &= \Big(-\frac{\mathrm{Re}[p_t]}{\mathrm{Re}[p_r]}, -\frac{\mathrm{Re}[p_t]}{\mathrm{Re}[p_\theta]}\Big). \end{aligned} \tag{14}$$

In the case of Fig. 1, the distribution of velocity $\boldsymbol{V}$ is shown in Fig. 2(a). The superscript + or − corresponds to the positive or negative sign of p_t in Eq. (11). The distributions of velocity in Fig. 2(a) are continuous about r, so the two branches + and − of multivalue function p_t correspond to two independent Riemann surfaces. Thus, the branch + (or −) are directly called mode + (or mode −) in this study. The value of $\boldsymbol{V}$ at $r = r_0$ has a good agreement with the velocity of fringes in our numerical simulation. Moreover, considering the singularity of velocity $\boldsymbol{\Lambda}$ at $r = r_0$, it is necessary to calculate its limit value by L'Hospital's rule. The new velocity of envelopes becomes

$$\tilde{\Lambda}_{(r)} = \frac{\partial_r G}{\partial_r H_{(r)}} = -\frac{\mathrm{Re}[p_{tr}]}{\mathrm{Re}[p_{rr}]}. \tag{15}$$

Its distribution on r is shown in Fig. 2(b). Its value at $r = r_0$ shows a good agreement with the velocity of envelopes measured in our numerical simulation.

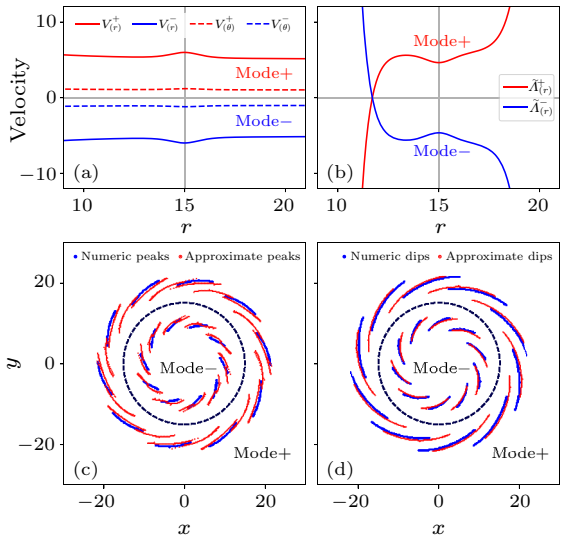

Fig. 2. (a) Dependence of fringes' velocity $\boldsymbol{V}$ on r. The red (or blue) solid and dashed curves denote the velocity in the directions of r and θ for mode + (or −), respectively. (b) Dependence of the envelopes' velocity $\tilde{\Lambda}_{(r)}$ on r. The red (or blue) curves correspond to mode + (or −). [(c), (d)] Distribution of (c) peaks and (d) dips of perturbation on the x–y plane when $t = 1$. The blue and red points are the results from numerical simulation and approximative solution (16), respectively. The dashed circle denotes $r = r_0$. The parameters are the same as those in Fig. 1.

As discussed above, there are two modes of dynamics when a perturbation is exerted on the plane wave background, which correspond to the two kinds of signs in the expression of p_t [see Eq. (11)]. The proportion (or amplitude) of different modes can be adjusted by the initial amplitudes A and B of perturbation. Assuming that the amplitudes of different components for mode + or − are denoted by $A^{\pm}$ and $B^{\pm}$, we have $A^+ + A^- = A$ and $B^+ + B^- = B$. Then we assume that $c^{\pm} = A^{\pm}/B^{\pm}$ is the proportion of two components, so

$$A^{\pm} = c^{\pm}B^{\pm}, \quad B^{\pm} = \pm(A - c^{\mp}B)/(c^+ - c^-).$$

They provide the amplitudes of perturbation for different modes, $A^+ + B^+$ and $A^- + B^-$. When B is a real number, $c^{\pm}$ can be calculated by $c^{\pm} = -c_{12}/c_{11}^{\pm}$, where $c_{11}^{\pm}$ corresponds to the cases with p_t for different modes [see Eq. (10)]. So far, one can construct an approximative solution to describe the perturbation's dynamics by combining the quantitative features and initial condition (6). Its expression can be given as follows:

$$\begin{aligned}\psi_{\mathrm{aprx}} = (&a_0 + A^+\mathrm{sech}[\eta_{(r)}E^+_{(r)}]\exp[ik_{(r)}F^+_{(r)} \\ &+ ik_{(\theta)}F^+_{(\theta)}] + B^+\mathrm{sech}[\eta_{(r)}E^+_{(r)}]\exp[-ik_{(r)}F^+_{(r)} \\ &- ik_{(\theta)}F^+_{(\theta)}] + A^-\mathrm{sech}[\eta_{(r)}E^-_{(r)}]\exp[ik_{(r)}F^-_{(r)} \\ &+ ik_{(\theta)}F^-_{(\theta)}] + B^-\mathrm{sech}[\eta_{(r)}E^-_{(r)}]\exp[-ik_{(r)}F^-_{(r)} \\ &- ik_{(\theta)}F^-_{(\theta)}])e^{-ia_0^2 t},\end{aligned} \tag{16}$$

where

$$\begin{aligned}&E^{\pm}_{(r)} = r - \tilde{\Lambda}^{\pm}_{(r)}t - r_0, \quad F^{\pm}_{(r)} = r - V^{\pm}_{(r)}t, \\ &F^{\pm}_{(\theta)} = \theta - V^{\pm}_{(\theta)}t,\end{aligned} \tag{17}$$

where $\tilde{\Lambda}^{\pm}_{(r)}$, $V^{\pm}_{(r)}$, and $V^{\pm}_{(\theta)}$ are the limit values of corresponding functions when $r = r_0$. This solution is effective for predicting the short-lived dynamics of perturbation. We show the peaks and dips of perturbation when $t = 1$ in Figs. 2(c) and 2(d), where the results of numerical simulation and the approximative solution are compared. They have a good agreement with each other. In the simulations, the peak (or dip) point is chosen when its density is larger (or smaller) than the points on its two sides in the direction of x or y. Note that the approximative solution (16) cannot describe the dynamics of perturbation after the derived inner ring arrives at its center. After that, the inner ring will cease to be ring-shaped and will converge into a complex localized structure. Then, it will expand and revert back to a ring-shaped structure, rotating toward the same direction as the initial ring. It will also have the same angular velocity as the initial ring, and the two rings will expand synchronously. As a result, its dynamical characters after arriving at the center can be predicted by mode +, instead of mode −, in the modified linear stability analysis. This is not beyond the applicable range of prediction, but the approximative solution (16) fails to describe the dynamics in this case.

The presence of the plane wave background is closely related to the appearance of reversal rotating mode (namely mode −). Thus, it is necessary to study the influence of background amplitude on the dynamics of perturbation. We define the relative amplitudes

of two modes as

$$S^{\pm} = \frac{A^{\pm} + B^{\pm}}{A + B}. \tag{18}$$

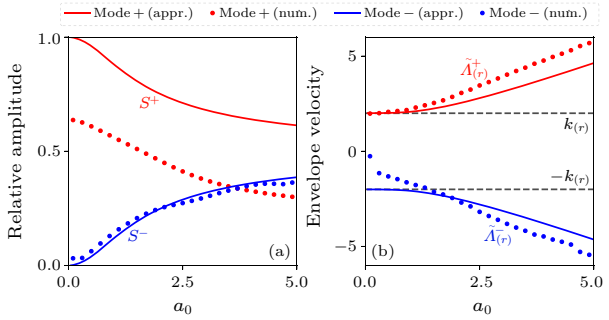

Fig. 3. Dependences of (a) the relative amplitude $S^{\pm}$ of perturbation and (b) the radial velocity $\tilde{\Lambda}^{\pm}_{(r)}$ of envelopes on the background amplitude a_0. The dotted and solid curves are the results of numerical simulation and approximative prediction [see Eqs. (15) and (18)]. The red and blue correspond to mode + and mode −, respectively. The black dashed lines denote the values of $\pm k_{(r)}$. The parameters are $a = 0.5$, $r_0 = 15$, $\eta_{(r)} = 1$, $k_{(r)} = 2$, $k_{(\theta)} = 10$.

The relation between them is $S^+ + S^- = 1$. When $a = 0.5$, $r_0 = 15$, $\eta_{(r)} = 1$, $k_{(r)} = 2$, and $k_{(\theta)} = 10$, the dependence of $S^{\pm}$ on background amplitude a_0 is shown in Fig. 3(a). When $a_0 = 0$, S^+ reaches its maximal value while S^- approaches 0. It means that mode − is suppressed and the perturbation keeps its initial mode. With a_0 increasing, S^+ decreases and S^- increases, which indicates the strong impact of background wave on the appearance of reverse rotation mode. In the numerical simulation, one can measure the maximal amplitude of wave outside (or inside) the circle $r = r_0$ and denote it by $|\psi|_{\text{out}}$ (or $|\psi|_{\text{in}}$). Thus, the numerical relative amplitude S^+ (or S^-) can be calculated by $(|\psi|_{\text{out}} - a_0)/a$ [or $(|\psi|_{\text{in}} - a_0)/a$], which is also shown in Fig. 3(a). By comparison, the prediction of Eq. (18) for S^- has a great agreement with the numerical results. However, there is a deviation between the two results for S^+. It may be caused by the decline of wave amplitude outside the circle $r = r_0$, maintaining the conservation of atom number during the spread of perturbation. In addition, according to Eq. (15), the influence of a_0 on the radial velocity of the envelopes is shown in Fig. 3(b). When $a_0 = 0$, its radial velocity $\tilde{\Lambda}^{\pm}_{(r)}$ is equal to $\pm k_{(r)}$, because the latter, i.e., the dimensionless momentum, is equal to the velocity. With a_0 increasing, the absolute value of $\tilde{\Lambda}^{\pm}_{(r)}$ becomes larger and larger. The radial velocity of the envelopes is measured in numerical simulations by the ratio of displacement of the point with density $|\psi|^2_{\text{out}}$ or $|\psi|^2_{\text{in}}$ to the time interval. Its results are also shown in Fig. 3(b). There is good agreement between the numerical and approximatively predicted results. Similar agreement can also be obtained when the contact interaction between atoms is attractive. In this case, there are two kinds of perturbation dynamics. The condition of them is related to the momentum of initial perturbation, which can be calculated by the traditional linear stability analysis. One of them is the modulation instability dynamics followed by the collapse of density peaks; the other is the splitting and reversely rotating dynamics shown in Fig. 1, whose dynamical characters can still be predicted by the modified linear stability analysis.

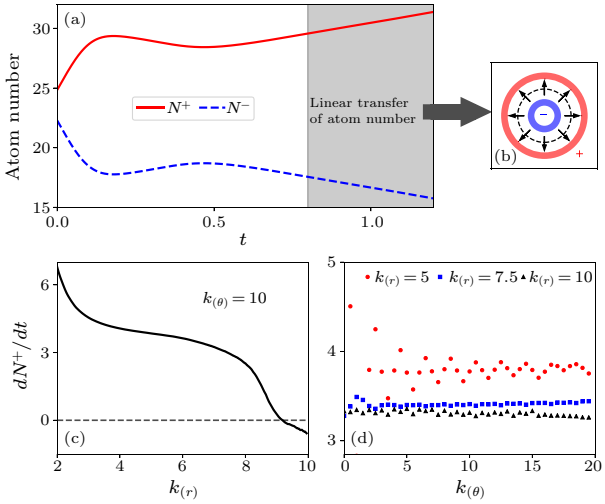

Fig. 4. (a) Change of perturbation atom number with time. The red solid and blue dashed curves denote the atom number of mode + and −, respectively. The atomic transfer between them is linear in the gray region. (b) Schematic of linear atomic transfer from mode − to mode +. (c) Influence of $k_{(r)}$ on the transfer rate dN^+/dt when $k_{(\theta)} = 10$. The gray dashed line denotes $dN^+/dt = 0$. (d) Influence of $k_{(\theta)}$ on dN^+/dt when $k_{(r)} = 5$ (red point), 7.5 (blue square), and 10 (black triangle). The other parameters are the same as Fig. 1.

Atomic Transfer between Rotating Rings. After the ring-shaped perturbation is exerted on the plane wave background, its reverse rotation mode is generated and the corresponding new ring appears, as shown in Fig. 1. The two rings gradually separate with time. A natural question comes up: is there the transfer of atom number between the two rings after they separate completely? Thus, we numerically measure the perturbation's atom number of two modes in the case of Fig. 1. The atom number of mode + or − is measured by the integral of perturbation's density outside or inside the circle $r = r_0$. They can be calculated by

$$N^+ = \int_{r_0}^{+\infty} \int_0^{2\pi} (|\psi|^2 - a_0^2)\, d\theta dr,$$
$$N^- = \int_0^{r_0} \int_0^{2\pi} (|\psi|^2 - a_0^2)\, d\theta dr. \tag{19}$$

The change of them with time is illustrated in Fig. 4(a). After the two rings separate almost completely, the atomic transfer between them becomes lin-

ear, which is obviously different from the one before separation. The schematic of linear atomic transfer is shown in Fig. 4(b), where the atoms are transferred from mode − to mode +. A possible cause of linear transfer is that, with the two rings separating, they take away the atoms from each other's regions, and the atom number taken away is constant in a contain time interval. Generally, the number of atoms taken away by the outside ring is larger than the one by the inside ring, which expresses as the atomic transfer from mode − to mode +. We calculate the rate of atomic transfer (denoted by dN^+/dt) by linear fitting in different cases, where the error of fitting is always much weaker than the value of transfer rate. The influence of $k_{(r)}$ on dN^+/dt is shown in Fig. 4(c). With the initial radial momentum $k_{(r)}$ increasing, the transfer rate dN^+/dt has an obvious decline. When $k_{(r)} \approx 9.2$, the atomic transfer almost ceases. When $k_{(r)} > 9.2$, we find $dN^+/dt < 0$, which means that the atoms are transferred from mode + to mode −. On the other hand, Fig. 4(d) illustrates the dependence of dN^+/dt on the initial angular momentum $k_{(\theta)}$. The transfer rate always has the fluctuation with changing $k_{(\theta)}$. When $k_{(r)} = 7.5$ and 10, the fluctuation is very weak, and the transfer rate has an almost constant distribution. When $k_{(r)} = 5$, the fluctuation gets stronger with $k_{(\theta)}$ decreasing. The inducement of fluctuation may be related to the expansion of the two rings. With $k_{(r)}$ decreasing, the two rings need more time to separate completely, so they have larger size due to their expansion. It means that they could distribute on each other's region and bring higher error for the calculation of the atom number $N^{\pm}$.

In summary, the dynamics of rotating ring-shaped perturbation on the plane wave in two-dimensional BECs is studied numerically. After the initial ring is exerted on the plane wave background, another ring emerges and moves away from the previous one, and the derived ring has the rotation whose direction is opposite to the previous one's. The derived ring becomes weaker and weaker with the background amplitude decreasing, and it vanishes in the case without the background. It indicates that the reversely rotating mode is closely related to the introduction of the plane wave background. Meanwhile, the modified linear stability analysis provides quantitative predictions on the dynamical features of two rings, like their velocity, amplitude, and frequency. These predictions inspire us to construct an approximative solution to describe the perturbation's dynamics. We compare the positions of perturbation's peaks and dips obtained by the approximative solution and numerical simulation, and the two results show good agreement. Furthermore, there is the transfer of atoms between the two rings, and the number of transferred atoms changes linearly with time after the two rings separate. It is found that the rate of transfer is greatly impacted by the initial radial momentum, instead of the initial angular one. Our results provide necessary reference for studies on the dynamics of 2D perturbed plane waves and illustrate the effectiveness of our analysis method in 2D nonlinear models. Considering the similarity of models of BECs and spatial optical material, our analysis may have broad applicability in the areas of spatial optics.

References

[1] Bradley C C, Sackett C A, Tollet J J and Hulet R G 1995 *Phys. Rev. Lett.* **75** 1687
[2] Bradley C C, Sackett C A and Hulet R G 1997 *Phys. Rev. Lett.* **78** 985
[3] Khaykovich L, Schreck F, Ferrari G, Bourdel T, Cubizolles J, Carr L D, Castin Y and Salomon C 2002 *Science* **296** 1290
[4] Strecker K E, Partridge G B, Truscott A G and Hulet R G 2002 *Nature* **417** 150
[5] Cornish S L, Thompson S T and Wieman C E 2006 *Phys. Rev. Lett.* **96** 170401
[6] Kevrekidis P G, Frantzeskakis D J and Carretero-González R 2007 *Emergent Nonlinear Phenomena in Bose-Einstein Condensates: Theory and Experiment* (Berlin: Springer) chap 1 p 4
[7] Zakharov V E and Shabat A B 1972 *Sov. Phys. JETP* **34** 62
[8] Song W W, Li Q Y, Li Z D and Fu G S 2010 *Chin. Phys. B* **19** 070503
[9] Liu X S, Ren Y, Yang Z Y, Liu C and Yang W L 2018 *Chin. Phys. Lett.* **35** 070501
[10] Zhao L C, Yang Z Y and Yang W L 2019 *Chin. Phys. B* **28** 010501
[11] Peregrine D H 1983 *Aust. Math. Soc. Ser. B* **25** 16
[12] Bludov Y V, Konotop V V and Akhmediev N 2009 *Phys. Rev. A* **80** 033610
[13] Akhmediev N, Ankiewicz A and Taki M 2009 *Phys. Lett. A* **373** 675
[14] Akhmediev N, Ankiewicz A and Soto-Crespo J M 2009 *Phys. Rev. E* **80** 026601
[15] Ankiewicz A, Kedziora D J and Akhmediev N 2011 *Phys. Lett. A* **375** 2782
[16] Guo B L, Ling L M and Liu Q P 2012 *Phys. Rev. E* **85** 026607
[17] He J S, Zhang H R, Wang L H, Porsezian K and Fokas A S 2013 *Phys. Rev. E* **87** 052914
[18] Kuznetsov E A 1977 *Sov. Phys. Dokl.* **22** 507
Ma Y C 1979 *Stud. Appl. Math.* **60** 43
[19] Akhmediev N and Korneev V I 1986 *Theor. Math. Phys.* **69** 1089
[20] Tajiri M and Watanabe Y 1998 *Phys. Rev. E* **57** 3510
[21] Zakharov V E and Gelash A A 2013 *Phys. Rev. Lett.* **111** 054101
[22] Ren Y, Yang Z Y, Liu C and Yang W L 2018 *Chin. Phys. B* **27** 010504
[23] Liu X S, Zhao L C, Duan L, Gao P, Yang Z Y and Yang W L 2018 *Chin. Phys. Lett.* **35** 020501
[24] Akhmediev N, Eleonskii V M and Kulagin N 1985 *J. Exp. Theor. Phys.* **61** 894
[25] Wu B, Liu J, Niu Q 2002 *Phys. Rev. Lett.* **88** 034101
[26] Dudley J M, Genty G, Dias F, Kibler B and Akhmediev N 2009 *Opt. Express* **17** 21497
[27] Zhao L C and Ling L 2016 *J. Opt. Soc. Am. B* **33** 850

[28] Trillo S and Wabnitz S 1991 *Opt. Lett.* **16** 986
[29] El G, Gurevich A, Khodorovskii V and Krylov A 1993 *Phys. Lett. A* **177** 357
[30] Biondini G and Mantzavinos D 2016 *Phys. Rev. Lett.* **116** 043902
[31] Mussot A, Naveau C, Conforti M, Kudlinski A, Copie F, Szriftgiser P and Trillo S 2018 *Nat. Photon.* **12** 303
[32] Conforti M, Li S, Biondini G and Trillo S 2018 *Opt. Lett.* **43** 5291
[33] Gerton J M, Strekalov D, Prodan I and Hulet R G 2000 *Nature* **408** 692
[34] Donley E A, Claussen N R, Cornish S L, Roberts J L, Cornell E A, Wieman C E 2001 *Nature* **412** 295
[35] Akhmediev N N, Heatley D R, Stegeman G I and Wright E M 1990 *Phys. Rev. Lett.* **65** 1423
[36] Chen S, Baronio F, Soto-Crespo J M, Grelu P and Mihalache D 2017 *J. Phys. A* **50** 463001
[37] Guo L, He J, Wang L, Cheng Y, Frantzeskakis D J, van den Bremer T S and Kevrekidis P G 2020 *Phys. Rev. Res.* **2** 033376
[38] He J, Song Y, Tiofack C G L and Taki M 2021 *Photon. Res.* **9** 643
[39] Caplan R M, Hoq Q E, Carretero-González R and Kevrekidis P G 2009 *Opt. Commun.* **282** 1399
[40] Afanasjev V V 1995 *Phys. Rev. E* **52** 3153
[41] Yang J 2010 *Nonlinear Waves in Integrable and Nonintegrable Systems* (Philadelphia: Siam) chap 7 p 332
[42] Gao P, Liu C, Zhao L C, Yang Z Y and Yang W L 2020 *Phys. Rev. E* **102** 022207
[43] Gao P, Duan L, Yao X, Yang Z Y and Yang W L 2021 *Phys. Rev. A* **103** 023519